Performance Validation of the Triangular Rollable and Collapsible Mast

Jeremy A. Banik & Thomas W. Murphey
Air Force Research Laboratory, Space Vehicles Directorate,
Kirtland AFB, NM 87117
Afrl.rvsv@kirtland.af.mil

ABSTRACT

A new deployable boom concept invented by AFRL has recently been gaining strong attention by those in the MicroSat and CubeSat communities. The Triangular Rollable And Collapsible (TRAC) mast has been demonstrated to enable new planar payloads and thus new mission concepts due to its extremely efficient packaging scheme. Several different material and geometric variations on the TRAC mast have been demonstrated to date. This mast can be engineered for either high packaging efficiency or high structural performance. The thinnest version is constructed from stainless steel allowing it to be packaged along with three other 4.0-meter long booms into a ½ U CubeSat volume. High structural performance versions are constructed of a carbon composite laminate that enable stiffer payloads such as a retractable 10m^2 solar sail. The deployed structural performance of these booms has been predicted and these models have been validated through structural testing.

INTRODUCTION

Tensioned planar structures are useful for a range of space missions including sunshades, solar sails, radar systems and photovoltaic arrays. DLR[1] has investigated a solar sail and radar architecture based on four booms that flatten and roll on a central hub, as shown in Figure 1. The DLR concept employs lenticular cross-section booms. While high in torsional stiffness due to their closed cross-section, lenticular architectures have the disadvantage of a relatively tall packaged height. On the other hand, the Triangular Rollable And Collapsible (TRAC)[2] mast uses an open cross-section to achieve a short packaged height. One application of the TRAC boom is to support the Flexible Unfurlable Refurlable Lightweight (FURL) Solar Sail[3] architecture represented in Figure 2.

Figure 3shows the deployed cross-section of three deployable boom architectures: (1) the Storable Tubular Extendable Member (STEM)[4,5], (2) the lenticular, which is sometimes referred to as the Collapsible Tubular Mast (CTM) and (3) the TRAC boom. All three booms can be stowed around a circular hub where they transition from a flattened configuration to a structurally deeper, deployed shape. The STEM is composed of a single strip that, in the deployed state, forms the circular cross-section shown in Figure 3(a). Although this configuration is simple to fabricate and package, it results in a large packaged height. The lenticular boom is made from a pair of symmetric bell shaped halves bonded at the edges shown in Figure 3(b). It flattens similar to a STEM, yet, its deployed geometry forms a closed section which is structurally efficient. For the same deployed cross-section circumference, the lenticular has half the packaged height as the STEM.

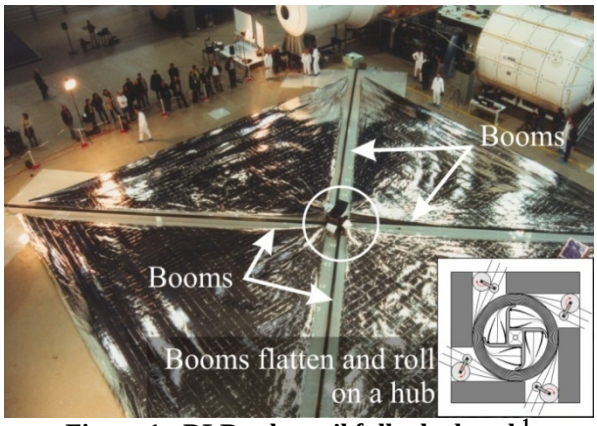

Figure 1: DLR solar sail fully deployed.[1]

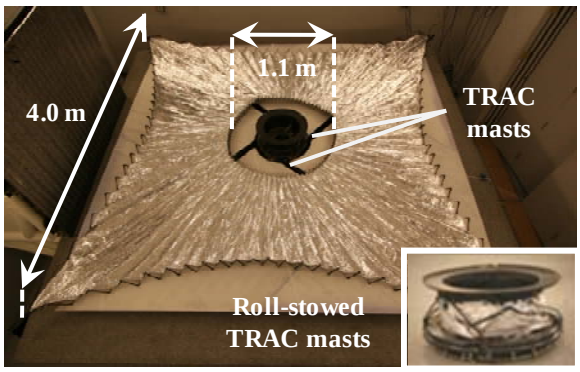

Figure 2: FURL solar sail fully deployed.[2,3]

The objective of this effort was to develop a boom architecture with large cross-section inertia to packaged height ratio compared to other similar boom architectures such as the STEM and CTM. TRAC's geometry was designed such that the boom flattens out to a height of 2.46 cm (0.97 in), as shown in Figure . Its deployed cross-section produces inertia properties of $I_x = 7.41 \times 10^{-10}$ m^4 (1.78×10^{-3} in^4) and $I_y = 4.99 \times 10^{-10}$ m^4 (1.2×10^{-3} in^4). For comparison, the cross-section inertia of each boom configuration were calculated assuming a packaged height of 2.46 cm and a maximum stowage strain of 1.5%. The STEM and lenticular effective diameters, D, were derived and their thicknesses were calculated assuming 1.5% strain (t/D). The resulting inertia properties are shown in Table 1. TRAC has 10 times more cross-section inertia for the same packaged height than the lenticular and 34 times more than the STEM.

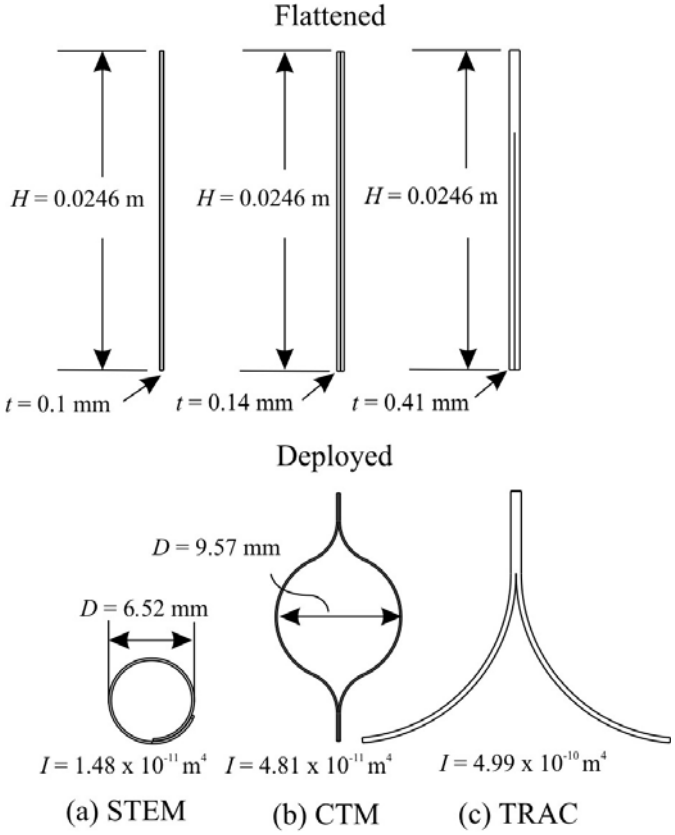

Figure 3: Deployable boom cross-sectional geometry

Table 1: TRACv1 cross section inertia calculations.

Boom Type	H (m)	t (mm)	D (mm)	I (m^4)
STEM	0.0246	0.1	H/1.2π = 6.52	$0.535D^3t = 1.48 \times 10^{-11}$
Lenticular or CTM	0.0246	0.14	H/2.57 = 9.57	$(\pi/8)D^3t = 4.81 \times 10^{-11}$
TRAC v1	0.0246	0.408	--	4.99×10^{-10}

This paper documents the prediction and measurement of TRAC's mechanical properties. The baseline design is discussed as well as the methods used to determine TRAC's geometry and material composition. A finite element analysis used to predict TRAC's stiffness and buckling strength properties is described. Tests to measure the boom's bending stiffness and strength are discussed and compared to the finite element analysis predictions. Finally, the performance of six different geometric variations of the TRAC boom are presented.

BOOM DESIGN

TRAC's structural material is carbon fiber reinforced polymer (CFRP) in uni-directional tape and plain weave fabric forms, both using Hexcel® IM7 fibers and 977-2 resin. The elastic properties assumed for this material system are given in Table 2. The weave properties were derived from the tape properties by modeling the weave as several perpendicular plies of tape.

Table 2: Material properties for unidirectional Hexcel® IM7/977-2 used in the FEM.

IM7 / 977-2 Unitape Pre-preg				
E_{11} (GPa)	E_{22} (GPa)	ν_{12}	ν_{23}	G_{12} (GPa)
173	9.17	0.34	0.37	5.65

The boom is designed such that in the stowed position its two flanges are pinched together allowing it to furl around a circular hub, as shown in Figure 4. The key to achieving this capability is that it is elastically stable in the pinched and rolled configuration. For example, the interior boom flange does not bifurcate from flat to open while in the rolled configuration. The stored strain energy from rolling counterbalances the stored energy from pinching for a certain range in roll diameters and flange radii. For example, bifurcation is sensitive to three parameters: the radius at which the boom is rolled, lateral bending stiffness when pinched, and symmetry about the horizontal centerline (i.e., all plies must be continuous from bottom to top). After several iterations of boom ply orientations, it was determined that the best stacking sequence to balance these effects is to sandwich a 45° weave between two or four 0° tape plies for each boom flange where 0° is the long axis of the boom. These two laminates overlap at the ridge to form either a [0°, ±45°, 0°, 0°, ±45°, 0°] stacking sequence or a [0°, 0°, ±45°, 0°, 0°, 0°, 0°, ±45°, 0°, 0°].

The flange radius, 0.0127 m (0.5 in), was selected for TRACv1. This radius dictates the boom wrap diameter must be less than 30.5 cm or else inner flange bifurcation will occur during wrapping. On the other hand, total laminate thickness (6 plies in this case) dictates the minimum wrap diameter must be greater than 18 cm or else fiber failure is likely during stowage.

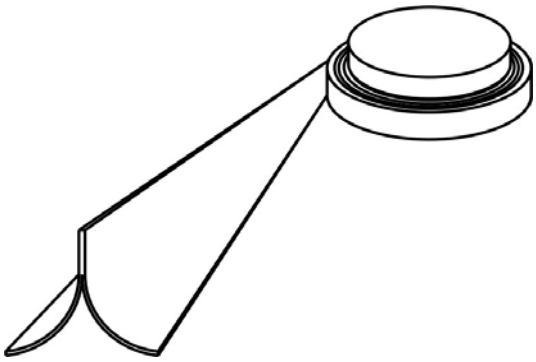

Figure 4: Deployment of the boom from the stowed position.

The disadvantage of the TRAC boom open cross-section design is low torsional stiffness. However, the thicker flange material allowed by the open section makes up for some of these stiffness losses. Also, preliminary load estimates revealed that the torsional stiffness of the boom is adequate for most applications.

A finite element model (FEM) of a 0.610 m (24 in) long TRACv1 boom was created using the ABAQUS finite element package and is shown in Figure 5. The nodes at the fixed end of the boom were fully constrained (encastre). The nodes at the free end were tied together (translations and rotations) to form a rigid cross-section. Enforced rotations were incrementally increased on a reference point coupled to the rigid cross-section to determine the boom's stiffness and strength properties.

The FEM was first used in a linear analysis design trade to optimize the boom's bending stiffness. From the enforced rotations, a resisting moment was calculated by the FEM solver and used to determine bending stiffness by the relation,

$$EI = \frac{ML}{\theta} . \qquad (1)$$

The flange flare angle was selected based on a design trade that tracked bending stiffness as a function of flange flare angle. The model was iterated between flare angles of 60^o to 170^o and determined *EI* in both x and y directions as defined the coordinate system in Figure 6. Results of the design trade are shown in Figure 7. The bending stiffnesses in the x and y directions do not converge, they plateau as flange flare angle is increased. To maximize the bending stiffness of the deployed cross-section while meeting the package height requirement, a flange flare angle of 170^o was selected for TRACv1.

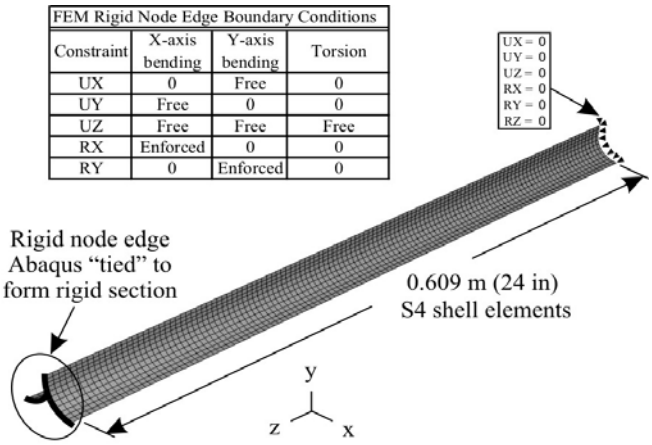

Figure 5: Boom finite element model boundary conditions.

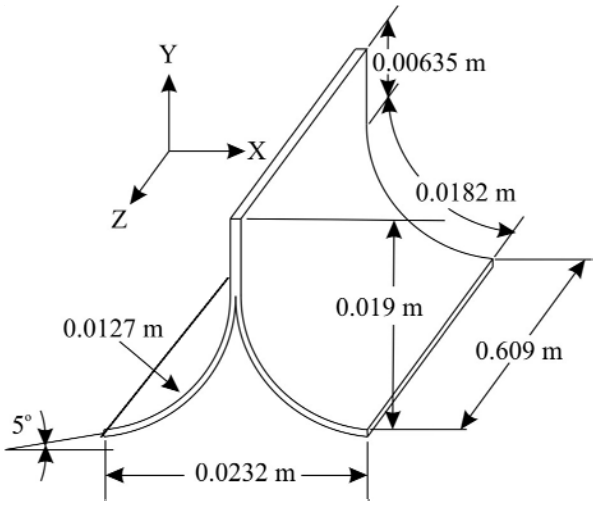

Figure 6: Dimensions of baseline design, TRACv1.

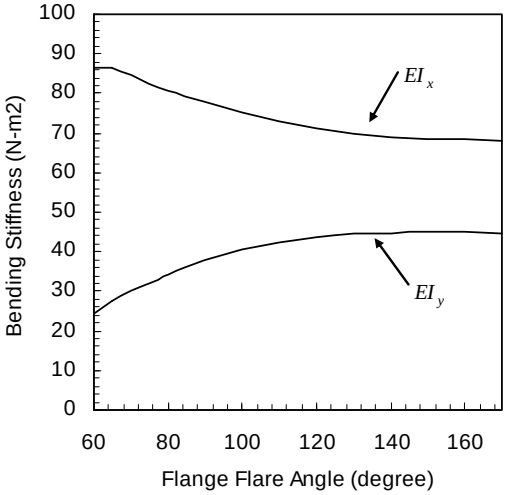

Figure 7: x and y axis bending stiffness as a function of flare angle for TRACv1.

TEST METHODOLOGY

The four-point bend test fixture shown in Figure 8 was engineered to characterize the test boom's bending stiffness about the x and y-axes. The test applies equal end moments so that the free length of boom is subjected to a uniform moment, as shown in Figure 9. Boom load pads are created by the addition of 0.394 m (5.50 in) extensions bonded to each end of the boom. These extensions enable a more precise application of moment to the specimen while eliminating stress concentrations and rotations that would occur by loading directly to the specimen surface. The two linear variable displacement transformers (LVDT) mounted at each end of the extensions are used to measure the rotation of the boom.

The testing fixture uses a stout beam to serve as a rigid reaction structure. Due to this tests sensitivity to small displacements, any bending of the base beam due to test loads could alter the results. The crosshead load acts through a rigid mount in the center of an I-beam, generating a pure moment at each end of the test boom. The angular rotation is measured by the two LVDTs mounted at each end of the test device (four total). The system is setup such that on each side of the pin/roller fulcrum there is an LVDT that measures vertical displacements shown in Figure 9 as δ_1 and δ_2. Angular rotation is then determined by,

$$\theta_L = \tan^{-1}\left(\frac{\delta_1 + \delta_2}{x_1 + x_2}\right), \qquad (2)$$

The total boom rotation is the sum of the rotations at the left and right ends, $\theta = \theta_L + \theta_R$. Assuming that the induced curvature is uniform, the boom radius of curvature R is measured by,

$$R = \frac{L}{\theta}, \qquad (3)$$

All bending tests used this procedure except for the x-axis bending buckling test with the V opening upwards. In this test, the displacements were larger than the range of the LVDTs and less accurate load frame load and displacement data was used.

Separate tooling was used to measure torsion, as shown in Figure 10. A moment was applied to the boom by counter wrapping a braided Dacron line around a hub attached to the base of the boom. A load frame was used to apply tensile loads to the cable and boom twist was calculated from the crosshead displacement data.

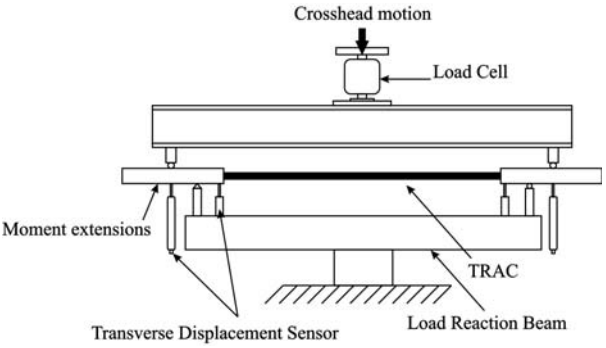

Figure 8: Schematic of four-point bend test device.

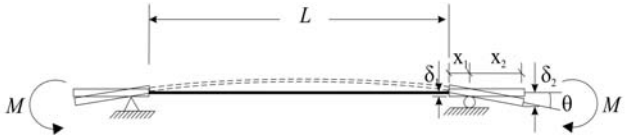

Figure 9: Four-point bend fixture displacements and measurements.

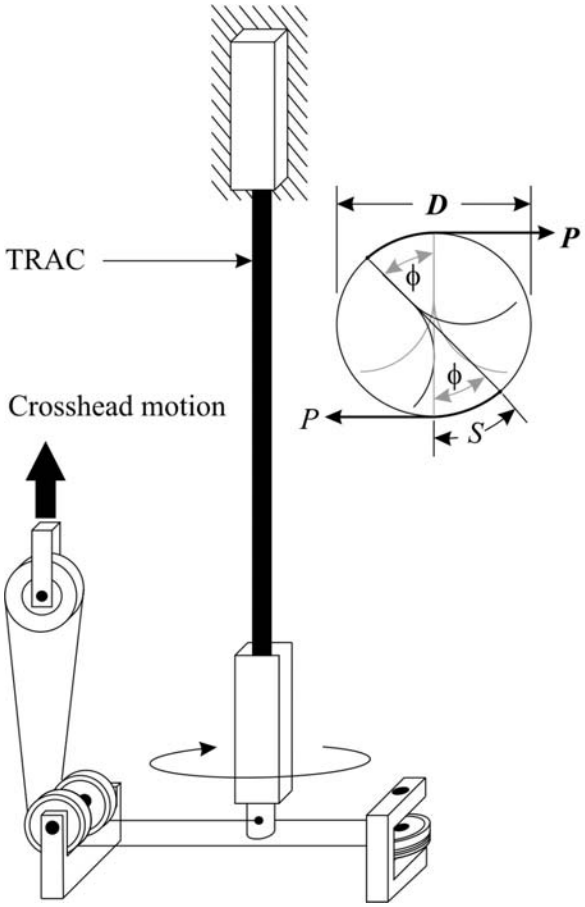

Figure 10: Schematic of the torsion test.

STRUCTURAL PERFORMANCE PREDICTIONS

The FEM described previously was used in nonlinear analyses to determine the boom's bending and torsional stiffness and buckling characteristics. Torsional stiffness was calculated using a method similar to the previous section. A boom twist was enforced at the reference point and the FEM analysis was used to solve for the reaction torque. The torsional stiffness was then determined by,

$$GJ = \frac{TL}{\phi}. \qquad (4)$$

Performance results from the tests and nonlinear FEM analyses on TRACv1 are shown in Figures 11 – 14.

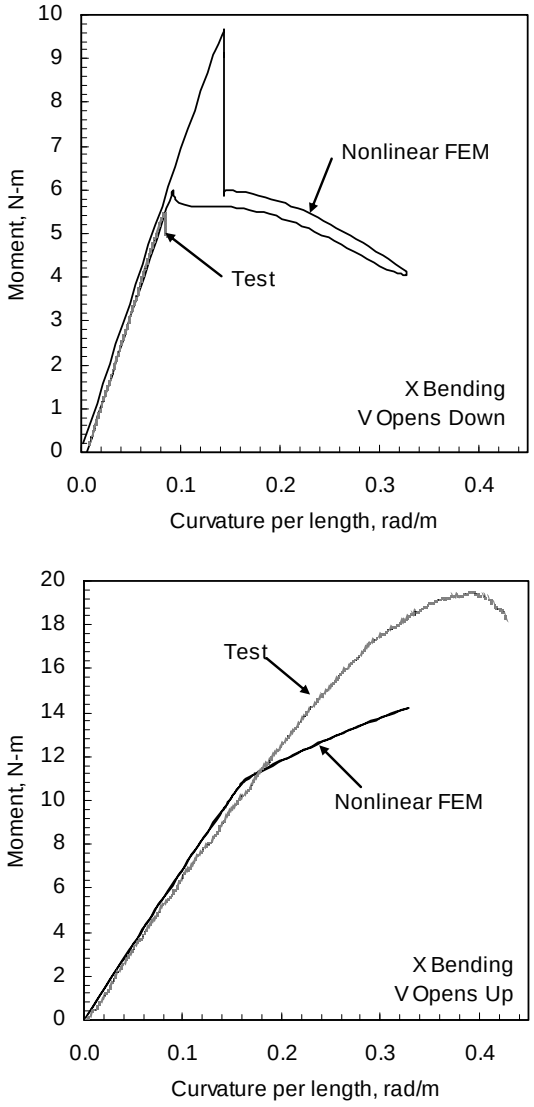

Figure 11: Nonlinear x axis bending FEM analysis and test results.

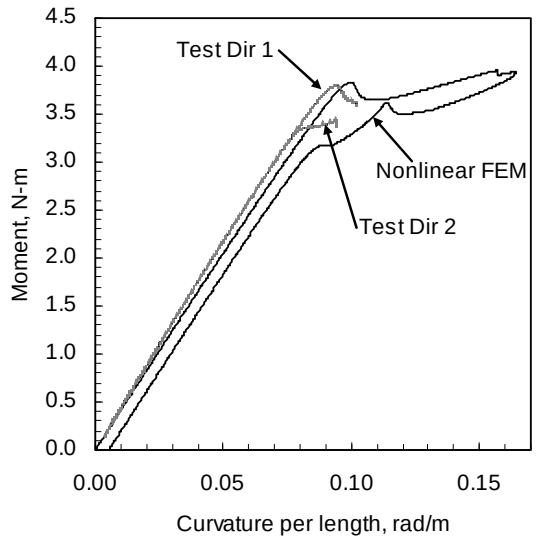

Figure 12: Nonlinear y axis bending FEM analysis and test results.

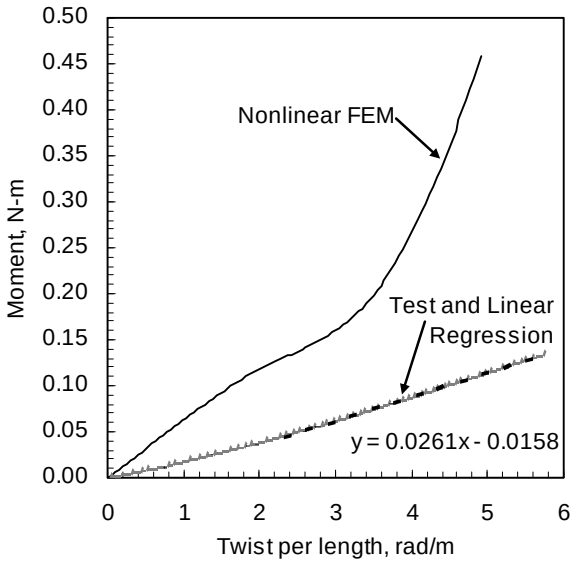

Figure 13: Nonlinear torsion FEM analysis and test results.

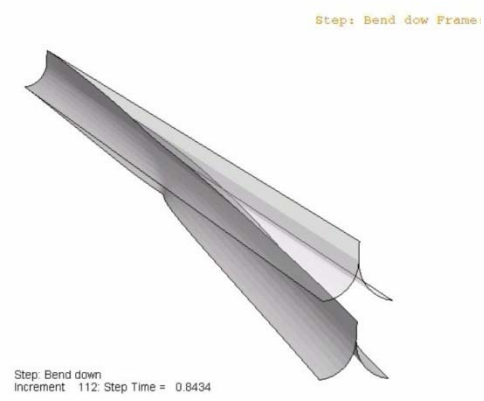

(a) FEM view of boom buckled with flanges facing downward

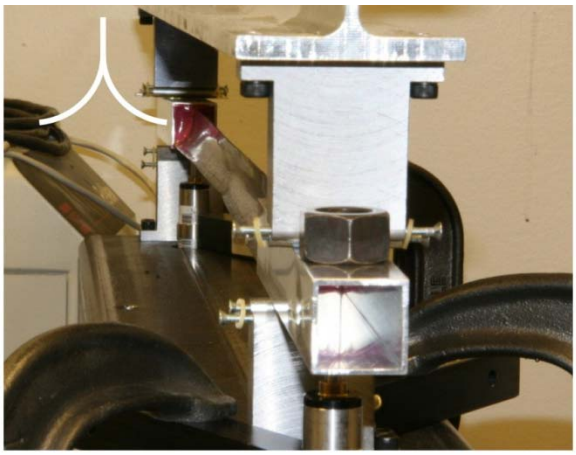

(b) Boom buckled with flanges facing downward

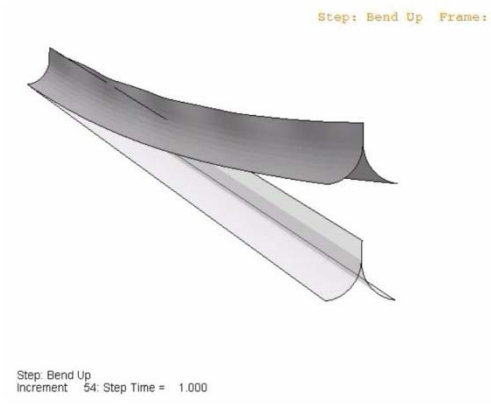

(c) FEM view of boom buckled with flanges facing upward

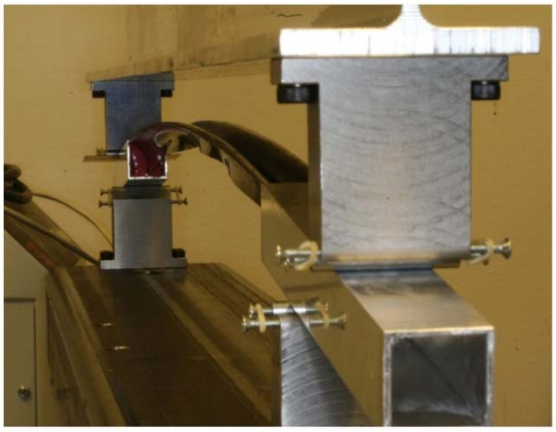

(d) Boom buckled with flanges facing upward

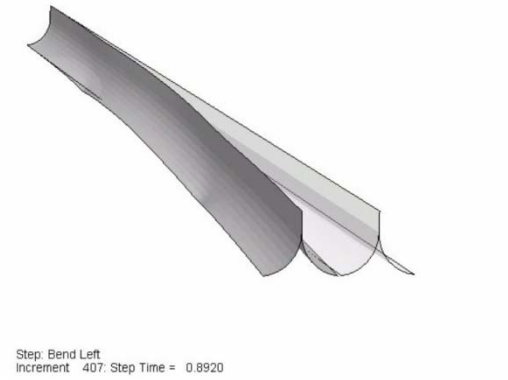

(e) FEM view of boom buckled with flanges facing north

(f) Boom buckled laying on its side with flanges facing north

Figure 14: Nonlinear FEM buckling mode shapes and corresponding buckling test photographs.

RESULTS AND DISCUSSION

Low loads were used during x and y-axis bending stiffnesses tests to avoid buckling and possible damage to the single test boom. The moment-curvature responses for these tests are shown in Figure 15, and linear regression calculated stiffnesses are summarized in Table 3. The stiffnesses measured in the two load directions for each axis are very similar. The x-axis stiffnesses differed by 1.7% with load direction and the y-axis stiffnesses differed by 0.9% with load direction. The test results are close to predictions with a 3.8% difference in the x-axis and a 6.5% difference in the softer y-axis. The boom exhibited no sign of buckling or laminate damage during loading and unloading.

A single test was used to measure torsional behavior because buckling was not expected. The results of this test are shown in Figure 13. The FEM predictions and test results differ significantly and there are two probable explanations for this. First, the boundary conditions used in the FEM fully constrained the motions of the boom except for translation along the long axis of the boom. The torsion test device, in contrast, allows for free translations in all directions and rotations about the x and y-axes. The test device constrains the boom less than the FEM and would be expected to result in a more compliant response. The FEM more accurately represents the accepted definition of torsional stiffness. Second, the line used as the torsion load path stretched significantly during the experiment. Subsequent tensile tests of the line showed nonlinear and non-repeatable stretches up to 1.2 cm at maximum test loads.

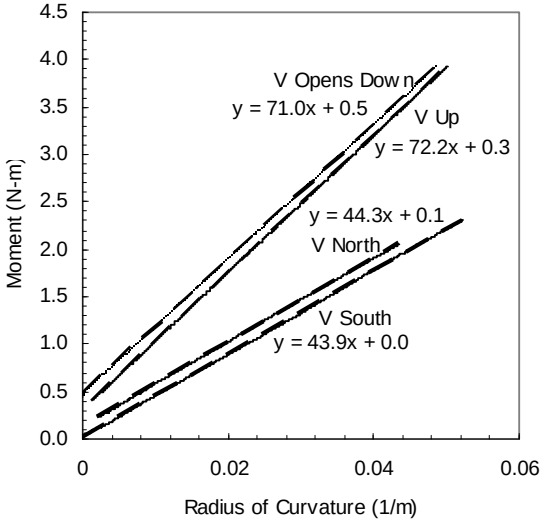

Figure 15: Moment-curvature response of stiffness bend tests.

Table 3: Nonlinear FEM stiffness and buckling load predictions and test results for TRACv1.

			Nonlinear FEM	Test	% Difference
x-axis bending	stiffness (*EIx*), N-m^2 (lb-in^2)		69.0 (24,042)	71.6 (24,949)	3.8
	V opens up	buckling load, N-m (in-lb)	10.5 (92.9)	19.5 (173)	85.7
	V opens down	buckling load, N-m (in-lb)	5.64 (49.9)	5.51 (48.8)	-2.3
y-axis bending	stiffness (*EIy*), N-m^2 (lb-in^2)		41.4 (14,422)	44.1 (15,367)	6.5
	buckling load, N-m (in-lb)		3.17 (28.1)	3.38 (29.9)	6.6
torsion	stiffness (*GJ*), N-m^2 (lb-in^2)		0.0643 (22.4)	0.0261 (9.09)	-59.4
	buckling load		No buckling at 4.9 rad/m	No buckling at 5.7 rad/m	--

Finally, buckling tests were performed using the bending test device. The moment-curvature results are shown in Figure 11 – 13 and the mode shapes are shown in Figure 14. The predicted and observed mode shapes and loads are similar. Flange buckling occurs when the boom is loaded such that the flange is in compression. The boom is 3.5 times stronger when the flanges are in tension and the thicker ridge is in compression. The boom does not buckle in torsional modes. The x-axis bending nonlinear FEM predicted an artificially high buckling load with increasing loading, however, upon reducing this load the FEM does not return to a un-buckled configuration until a much lower load is reached. This lower load corresponds to the buckling load observed during testing.

Once the finite element techniques had been validated by test data; thicker laminates, taller packaged sizes, larger flange radii geometries, and even alternate materials were explored. Table 4 lists the six different TRAC boom versions that have been fabricated and demonstrated to date. The structural performance metrics listed are based on non-linear FEM predictions unless specifically indicated to be test results. Note that TRACv4 performs well for a small wrap diameter of 18 cm. The TRACv5 has the highest structural performance of all versions but at the penalty of a larger minimum wrap diameter of 28 cm. Also note that the stainless steel version TRACvSS can be wrapped to a very small diameter of 3.8 cm, making this version an attractive solution for CubeSats. In general the maximum wrapped diameter is driven by inner flange buckling and the minimum is driven by fiber failures.

Table 4: Six different geometric and material variations of the TRAC boom have been fabricated and demonstrated to date. Performance predictions are based on non-linear FEM of a 0.61 m section.
Denotes test results.

	Material	*Stowed Height* (cm)	*Flange Radius* (cm)	*Total Thickness* (mm)	*Min. Wrap Dia.* (cm)	*Max. Wrap Dia. (cm)*	*EIx* ($N\text{-}m^2$)	*EIy* ($N\text{-}m^2$)	*GJ* ($N\text{-}m^2$)	*Critical Load, Mx (N-m)*	*Critical Load, My (N-m)*
TRACv1	[0, 45PW, 0]s	2.46	1.27	0.91	18	30.5*	71.6*	44.1*	0.064	5.51*	3.38*
TRACv2	[0, 45PW, 0]s	3.81	4.32	0.91	18	82*	312	179	0.073	--	1.90
TRACv3	[0, 0, 45PW, 0, 0]s	3.81	4.32	1.40	28	82*	747	168	0.141	12.9	6.30
TRACv4	[0, 45PW, 0]s	3.81	2.54	0.91	18	56*	254	304	0.080	10.3	8.05
TRACv5	[0, 0, 45PW, 0, 0]s	3.81	2.54	1.40	28	56	474	578	0.169	31.5	16.7
TRACvSS	Stainless Steel	3.43	1.8	0.1	3.8	10*	57.2	84.0	0.131	1.85	1.61

CONCLUSIONS

The present investigation was conducted to evaluate the performance of a new deployable boom called the TRAC. The efforts focused on the development of a design that maximizes stiffness while maintaining the ability to flatten and furl around a circular hub. During the course of this investigation finite element analyses were employed to aid in developing a baseline design.

Exploration of different CFRP laminates yielded discovery of a stacking sequence that utilized symmetry while maintaining a specific cross-sectional flange radius and lateral stiffness. A test boom was fabricated and subjected four-point bend tests and torsional tests to measure its moment-curvature and twist response. Tests correlated well with the finite element predictions for all bending tests. The torsion tests did not correlate with predictions and probable causes for this were discussed.

The close correlation between FEM and test results provides evidence the bending characteristics of a TRAC boom are predictable and well understood. Industry standard nonlinear FEM tools accurately predict the behavior of the boom. This strong correlation increases confidence that FEMs of larger and longer TRAC booms, as components of a system model, will also be accurate. In fact, these analysis tools were used to predict performance of six different variations on the TRAC boom, all of which have been successfully fabricated to date.

The thinnest version of the TRAC boom has recently been implemented as the main structural support for two independent CubeSat payloads, LightSail-I and NanoSail-D2. NanoSail-D2[6] is a $10m^2$ solar sail that uses four 2.2-meter TRACvSS booms and is scheduled to launch in the fall of 2010. LightSail-I[7,8] is a larger sail that uses four 4-meter TRACvSS booms and is currently in preparation for a 2011 launch. Both boom systems package into 10 x 10 x 5 cm volume.

References

1. Leipold, M., Runge, H., Sickinger, C., "Large SAR Membrane Antennas with Lightweight Deployable Booms," 28th ESA Antenna Workshop on Space Antenna Systems and Technologies, ESTEC, Noordwijk, 2005.
2. Murphey, T. W., Banik, J. A., "Triangular Rollable and Collapsible Boom," U.S. Patent Pending 11876081.
3. Banik, J., Ardelean, E., "Verification of a Retractable Solar Sail in a Thermal-Vacuum Environment." 51st AIAA Structures, Structural Dynamics, and Materials Conference, 2010-2585, Orlando, Florida, 2010.
4. Rimrott, F.P.J, "Storable Tubular Extendable Member - A Unique Machine Element," Journal of Machine Design, Vol. 37, pg. 156-165, 1965.
5. Hazelton, C.S., Gall, K.R., Abrahamson, E.R., Denis, R.J., Lake, M.S., "Development of a Prototype Elastic Memory Composite (STEM) for Large Space Structures," AIAA paper 2003-1977.
6. Whorton, M., Heaton, A., Pinson, R., Laue, G., Adams, C., "NanoSail-D: The First Flight Demonstration of Solar Sails for Nanosatellites," 22nd AIAA/USU Conference on Small Satellites, SSC08-X-1, Logan, Utah. 2008.
7. "Projects: LightSail - The Future of Solar Sailing," Planetary Society projects page. http://www.planetary.org/programs/projects/solar_sailing/lightsail1.html. Retrieved on 26 Feb 2010.
8. Friedman, L., "Lightsail Update:" *Planetary Report*. Vol. XXX, No. 3, May/June 2010. pp 4-7.